Diabetes promotes an inflammatory macrophage phenotype and atherosclerosis through acyl-CoA synthetase 1

Jenny E. Kanter[a], Farah Kramer[a], Shelley Barnhart[a], Michelle M. Averill[a], Anuradha Vivekanandan-Giri[b], Thad Vickery[c], Lei O. Li[d], Lev Becker[e], Wei Yuan[e,1], Alan Chait[e], Kathleen R. Braun[f], Susan Potter-Perigo[f], Srinath Sanda[g], Thomas N. Wight[f], Subramaniam Pennathur[b], Charles N. Serhan[c], Jay W. Heinecke[e], Rosalind A. Coleman[d], and Karin E. Bornfeldt[a,2]

[a]Department of Pathology, Diabetes and Obesity Center of Excellence, University of Washington School of Medicine, Seattle, WA 98109; [b]Department of Internal Medicine, University of Michigan, Ann Arbor, MI 48109; [c]Center of Experimental Therapeutics, Department of Anesthesiology, Perioperative and Pain Medicine, Brigham and Women's Hospital, Harvard Medical School, Boston, MA 02115; [d]Department of Nutrition, University of North Carolina, Chapel Hill, NC 27599; [e]Department of Medicine, Diabetes and Obesity Center of Excellence, University of Washington School of Medicine, Seattle, WA 98109; and [f]Hope Heart Matrix Biology Program and [g]Diabetes Research Program, Benaroya Research Institute at Virginia Mason, Seattle, WA 98101

Edited* by Joseph A. Beavo, University of Washington School of Medicine, Seattle, WA, and approved December 8, 2011 (received for review July 17, 2011)

The mechanisms that promote an inflammatory environment and accelerated atherosclerosis in diabetes are poorly understood. We show that macrophages isolated from two different mouse models of type 1 diabetes exhibit an inflammatory phenotype. This inflammatory phenotype associates with increased expression of long-chain acyl-CoA synthetase 1 (ACSL1), an enzyme that catalyzes the thioesterification of fatty acids. Monocytes from humans and mice with type 1 diabetes also exhibit increased ACSL1. Furthermore, myeloid-selective deletion of ACSL1 protects monocytes and macrophages from the inflammatory effects of diabetes. Strikingly, myeloid-selective deletion of ACSL1 also prevents accelerated atherosclerosis in diabetic mice without affecting lesions in nondiabetic mice. Our observations indicate that ACSL1 plays a critical role by promoting the inflammatory phenotype of macrophages associated with type 1 diabetes; they also raise the possibilities that diabetic atherosclerosis has an etiology that is, at least in part, distinct from the etiology of nondiabetic vascular disease and that this difference is because of increased monocyte and macrophage ACSL1 expression.

It is becoming increasingly clear that monocytes isolated from humans with type 1 diabetes display an inflammatory phenotype and secrete higher levels of proinflammatory cytokines, such as IL-6 and IL-1β, than do monocytes from subjects without diabetes (1–5). Furthermore, inflammatory monocytes found in the setting of type 1 diabetes have recently been shown to result in Th17 cell activation (2, 6), suggesting that the proinflammatory effect of diabetes on monocytes/macrophages may result in wide-ranging effects on the immune system. Monocytes and macrophages are centrally important in atherogenesis and may play critical roles in diabetes-accelerated cardiovascular disease (7) and other complications of diabetes. Atherosclerotic vascular disease is the leading cause of death among people with types 1 and 2 diabetes, but this greatly increased incidence cannot be completely explained by the traditional cardiovascular risk factors. Systemic factors, such as dyslipidemia, hyperglycemia, hypertension, microalbuminuria, and low-grade inflammation, are often viewed as culprits in diabetic vascular disease. For example, clinical studies suggest that suboptimal glycemic control early in the cardiovascular disease progression promotes cardiovascular events later in life in subjects with type 1 diabetes (8). This hypothesis is supported by studies on animal models of the disease (9–11).

One viewpoint that has gained increased traction is that direct effects of diabetes on atherosclerotic lesion cells, such as macrophages, play an additional important role (12). Thus, the increased macrophage expression of inflammatory mediators associated with diabetes can be mimicked by elevated glucose concentrations in vitro (13). In addition, fatty acids exert inflammatory effects in macrophages, which could contribute to inflammation in the setting of diabetes (14), diabetes-accelerated atherosclerosis, and possibly other complications. After entering the cell, these fatty acids are thioesterified into their acyl-CoA derivatives, a process catalyzed by long-chain acyl-CoA synthetases (ACSLs).

In the current studies, we investigated the potential link between ACSL and diabetes in macrophages and monocytes. We show that ACSL1, an enzyme that hitherto has been implicated only in fatty acid incorporation into cellular lipids and use for β-oxidation, is up-regulated in monocytes and macrophages by type 1 diabetes, concomitant with well-known inflammatory mediators. Furthermore, myeloid-targeted deletion of ACSL1 inhibits the inflammatory activation of macrophages in the setting of diabetes and prevents diabetes-accelerated atherosclerosis in an established mouse model of type 1 diabetes. Our observations show that ACSL1 is centrally and selectively important in mediating the inflammatory phenotype of macrophages associated with diabetes.

Results

Diabetes Results in an Inflammatory Macrophage Phenotype Characterized by Increased ACSL1 Expression and Increased Arachidonoyl-CoA Levels. Monocytes isolated from human subjects with type 1 diabetes exhibit increased secretion of proinflammatory cytokines (1, 2). Using a transgenic mouse model of type 1 diabetes, in which T-cell–mediated destruction of pancreatic β-cells expressing a viral glycoprotein (GP) can be induced at will by lymphocytic choriomeningitis virus (LCMV) injection (10), we investigated if diabetes promotes a proinflammatory state in macrophages. LCMV-injected low-density lipoprotein receptor $(LDLR)^{-/-}$;GP^{+} mice were hyperglycemic (Fig. 1*A*) but showed no significant changes in blood cholesterol (Fig. 1*B*) compared with saline-injected $LDLR^{-/-}$;GP^{+} mice or LCMV-injected $LDLR^{-/-}$ mice without the GP transgene (Fig. S1 *A* and *B*). In both resident and thioglycollate-

Author contributions: J.E.K., L.B., C.N.S., and K.E.B. designed research; J.E.K., F.K., S.B., M.M.A., A.V.-G., T.V., L.O.L., L.B., K.R.B., and S.P.-P. performed research; W.Y., A.C., S.S., T.N.W., J.W.H., and R.A.C. contributed new reagents/analytic tools; J.E.K., L.B., S.S., S.P., and K.E.B. analyzed data; and J.E.K. and K.E.B. wrote the paper.

The authors declare no conflict of interest.

*This Direct Submission article had a prearranged editor.

[1]Present address: Center for Advanced Research in Biotechnology, University of Maryland Biotechnology Institute, Rockville, MD 20850.

[2]To whom correspondence should be addressed. E-mail: bornf@uw.edu.

See Author Summary on page 4353 (volume 109, number 12).

This article contains supporting information online at www.pnas.org/lookup/suppl/doi:10.1073/pnas.1111600109/-/DCSupplemental.

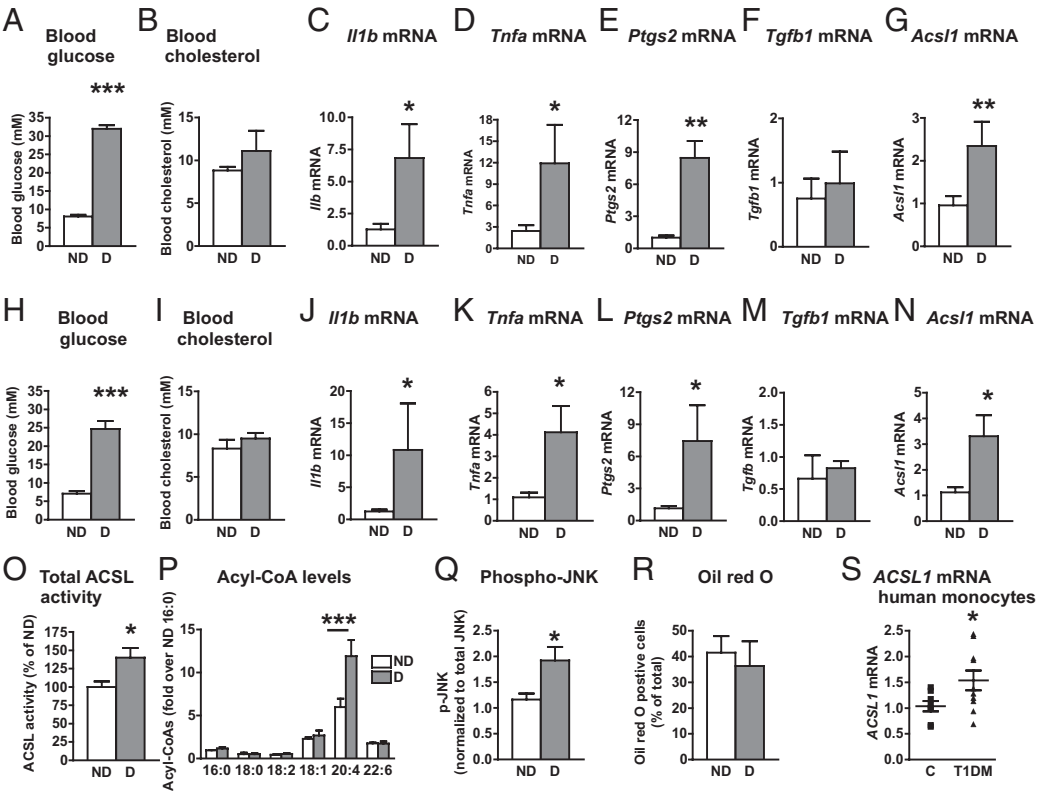

Fig. 1. Diabetes promotes an inflammatory macrophage phenotype characterized by increased ACSL1 expression. (*A–G*, *O*, and *R*) LDLR$^{-/-}$;GP^{+} (n = 5–7) mice were injected with LCMV or saline; alternatively (*H–N*, *P*, and *Q*), LDLR$^{-/-}$;GP^{+} mice (n = 6–9) were injected with streptozotocin (STZ) or citrate buffer (control). All mice were maintained on a low-fat diet for 4 wk after the onset of diabetes. At the end of 4 wk, blood glucose (*A* and *H*) and blood cholesterol (*B* and *I*) were measured, and peritoneal macrophages were harvested by lavage. Real-time qPCR was used to determine abundance of pro- and antiinflammatory markers. (*C* and *J*) *Il1b* mRNA, (*D* and *K*) *Tnfa* mRNA, (*E* and *L*) *Ptgs2* mRNA, (*F* and *M*) *Tgfb1* mRNA, and (*G* and *N*) *Acsl1* mRNA. Similar results were obtained from thioglycollate-elicited and resident macrophages. (*O*) Total ACSL enzymatic activity measured as the rate of conversion of [^{3}H]-18:1 to [^{3}H]-18:1-CoA in thioglycollate-elicited macrophages. (*P*) Acyl-CoA species measured by LC-ESI-MS/MS. (*Q*) Phospho-JNK levels were measured by Western blot and normalized to total levels of JNK in thioglycollate-elicited macrophages (n = 4–5). (*R*) Oil red O staining of thioglycollate-elicited macrophages. (*S*) CD14+ monocytes were isolated from human subjects with type 1 diabetes or age-matched controls. *ACSL1* mRNA was measured by real-time qPCR (n = 8–9). The results are expressed as mean + SEM or scatter plots. *$P < 0.05$, **$P < 0.01$, and ***$P < 0.001$ by unpaired Student t test compared with nondiabetic controls. Levels of mRNA are expressed as fold-over nondiabetic controls. When statistically justified, mRNA levels were log-transformed before statistical analysis was performed. ND, nondiabetic mice; D, diabetic mice; T1DM, human subjects with type 1 diabetes mellitus; C, control.

elicited macrophages from diabetic mice, there was a clear increase in mRNA levels of inflammatory mediators, including *Il1b* (Fig. 1*C*), *Tnfa* (Fig. 1*D*), and prostaglandin-endoperoxide synthase 2 (*Ptgs2*) or cyclooxygenase 2 (Fig. 1*E*), compared with macrophages from nondiabetic littermates. Additionally, consistent with the elevated *Ptgs2* levels, macrophages from diabetic mice secreted increased levels of prostaglandin (PG) E_2 (319.8 ± 57.4 pg/2 × 10^6 cells from diabetic mice vs. 179.6 ± 19.2 pg/2 × 10^6 cells from nondiabetic mice, n = 4–5, $P < 0.05$). Conversely, there were no significant changes in mRNA levels of the anti-inflammatory mediator *Tgfb1* (Fig. 1*F*). The increased macrophage proinflammatory status could not be explained by LCMV injection per se (Fig. S1 *C–F*). Interestingly, *Acsl1* mRNA was also up-regulated in macrophages from animals with diabetes (Fig. 1*G*).

To investigate if these results could be confirmed in another model of type 1 diabetes, we analyzed thioglycollate-elicited peritoneal macrophages from streptozotocin diabetic mice and nondiabetic littermates. Consistent with the data on the LDLR$^{-/-}$;GP model, streptozotocin diabetic mice had elevated blood glucose levels (Fig. 1*H*) without differences in blood cholesterol levels (Fig. 1*I*). Furthermore, peritoneal macrophages harvested from streptozotocin diabetic mice showed a similar increase in *Il1b*, *Tnfa*, and *Ptgs2*, which associated with an increase in *Acsl1* mRNA (Fig. 1 *J–N*). In addition, total ACSL enzymatic activity was significantly up-regulated in macrophages from diabetic mice (Fig. 1*O*), and this up-regulation resulted in a selective increase in arachidonoyl-CoA (20:4-CoA) levels as measured by liquid chromatography electrospray ionization tandem MS (LC-ESI-MS/MS) (Fig. 1*P*). At the level of signal transduction, phosphorylation of JNK was increased in thioglycollate-elicited macrophages from diabetic mice (Fig. 1*Q*), further supporting the evidence of an inflammatory macrophage phenotype. Thus, ACSL1 expression correlates with an inflammatory macrophage phenotype and increased 20:4-CoA levels in diabetes.

Other studies have implicated ACSL1 in neutral lipid accumulation in cells (15–18); however, the increased ACSL1 in macrophages from diabetic mice was not associated with increased macrophage neutral lipid loading, which was assessed by oil red O staining (Fig. 1*R*).

Next, we isolated CD14^{+} monocytes from human subjects with type 1 diabetes 528 ± 168 d within its onset and age-matched controls (patients with diabetes were 28.6 ± 3.1 y and controls were 30.2 ± 3.9 y, P = 0.74, n = 9 and n = 8, respectively). The subjects with diabetes were on insulin therapy, but they did not take any other medication and did not have complications of diabetes. Although a relatively small number of matched human subjects were analyzed, the results show that, consistent with the

data from the two mouse models, human subjects with type 1 diabetes had significantly elevated levels of *ACSL1* mRNA in monocytes (Fig. 1*S*).

In summary, diabetes induces inflammatory changes in mouse macrophages concomitant with up-regulation of ACSL1 in the absence of neutral lipid accumulation or changes in plasma lipid levels. A similar up-regulation of ACSL1 is present in $CD14^+$ monocytes from human subjects with type 1 diabetes.

ACSL1 Is Up-Regulated in Highly Inflammatory Mouse and Human Macrophages. To investigate whether the reason for up-regulation of ACSL1 in macrophages by diabetes could be because of inflammation, we used the well-established highly inflammatory macrophage population induced by LPS and IFN-γ in vitro (commonly referred to as M1 activation) (19). Mouse bone marrow-derived macrophages (BMDMs) were differentiated using macrophage colony-stimulating factor (M-CSF) and then activated into M1 macrophages. Interestingly, ACSL1 was markedly up-regulated in M1 macrophages compared with unactivated controls. This up-regulation of ACSL1 was evident at the *Acsl1* mRNA level (Fig. 2*A*), ACSL1 protein level ($P < 0.05$), and plasma membrane-associated ACSL1 (Fig. 2*B*). IL-4 stimulation (M2 activation) did not up-regulate ACSL1 (Fig. 2*B*). Furthermore, insulin did not regulate ACSL1 expression in macrophages under unactivated basal or M1 conditions (M1 stimulation resulted in a 5.5 ± 0.6-fold increase in *Acsl1* mRNA in the absence of insulin and a 5.3 ± 0.4-fold increase in the presence of 10 nM insulin, $n = 3$, $P = 0.74$).

We next investigated whether human macrophages would respond with an increase in *ACSL1* to inflammatory conditions. Like mouse BMDMs, human monocyte-derived macrophages exhibited a significant increase in *ACSL1* mRNA after M1 stimulation compared with unactivated controls (Fig. 2*C*), and this increase was associated with a significant increase in plasma membrane-associated ACSL1 (Fig. 2*D*). Inflammatory activation, therefore, up-regulates ACSL1 both in mouse and human macrophages.

Generation of a Myeloid-Selective ACSL1-Deficient Mouse Model. We next generated a mouse model with myeloid-specific ACSL1 deficiency (Fig. 3*A*), which is referred to as the $ACSL1^{M-/-}$ (myeloid-selective ACSL1-deficient) mouse. *Acsl1* mRNA levels were markedly reduced in macrophages from $ACSL1^{M-/-}$ mice compared with wildtypes (WTs) (Fig. 3*B*). ACSL1 protein (Fig. 3*C*) and total ACSL enzymatic activity were significantly reduced in $ACSL1^{M-/-}$ macrophage lysates (Fig. S2*A*) but not in liver (Fig. S2*B*), showing tissue selectivity of the ACSL1 deletion. ACSL1 is a predominant ACSL isoform in mouse macrophages (20). The finding that ACSL1 deficiency reduced total ACSL activity by ∼45% (Fig. S2*A*) suggests that other ACSL isoforms or other enzymes with ACSL activity make up the remaining ∼55% of oleoyl-CoA synthetase activity in isolated macrophages. Importantly, there was no compensatory up-regulation of gene expression of other ACSL isoforms in ACSL1-deficient macrophages (Fig. S2 *C* and *D*). Thus, the $ACSL1^{M-/-}$ mouse exhibits a marked loss of ACSL1 in macrophages.

ACSL1 Deficiency Does Not Impair Macrophage Neutral Lipid Accumulation in Vivo. ACSL1 has been implicated in neutral lipid accumulation (15–18) and β-oxidation pathways (21) in liver and adipose tissue. Accordingly, ACSL1-deficient macrophages challenged with oleate (18:1) in vitro exhibited defects in 18:1 partitioning into neutral lipids and increased levels of cellular free 18:1, but they showed no changes in 18:1 β-oxidation (Fig. S2 *E–H*). Furthermore, total cellular levels of free and esterified cholesterol or free fatty acids were not altered by

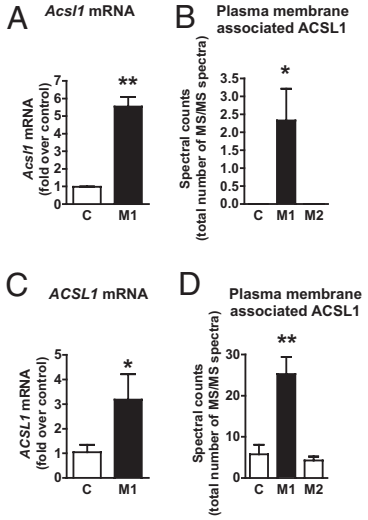

Fig. 2. ACSL1 is markedly increased in inflammatory macrophages. Mouse BMDMs from WT mice were activated using LPS/IFN-γ (for M1 polarization) or IL-4 (for M2 polarization) or were left as unactivated controls for 48 h. (*A*) *Acsl* mRNA levels were measured by real-time qPCR. (*B*) Plasma membranes isolated from biotin-labeled M1 and M2 macrophages and unactivated macrophages (controls) were subjected to LC-MS/MS. The spectral counts represent the total number of ACSL1-derived peptides identified ($n = 6$). (*C*) Human monocyte-derived macrophages were differentiated in the presence of M-CSF and then activated with LPS/IFN-γ (M1) or left unactivated (control). *ACSL1* mRNA was measured by real-time qPCR ($n = 3$–5). (*D*). Membrane-associated ACSL1 in human monocyte-derived macrophages was measured by Western blot or LC-MS/MS as described for mouse BMDMs. The results are expressed as mean + SEM ($n = 3$ unless otherwise noted). $^*P < 0.05$ and $^{**}P < 0.01$ by unpaired Student *t* test. C, control.

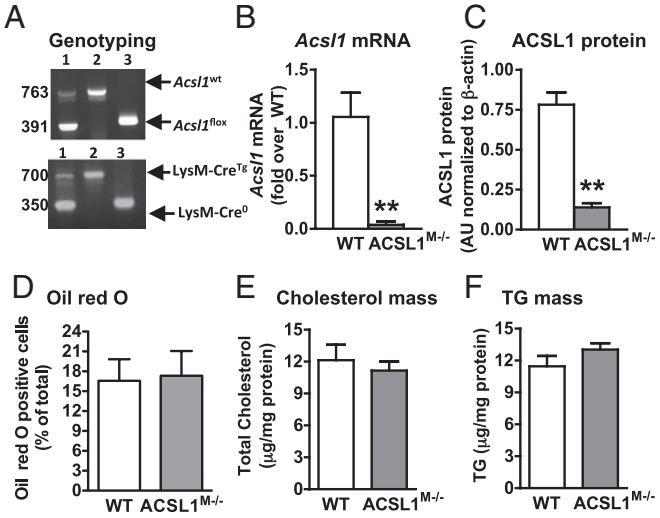

Fig. 3. Generation of a myeloid-selective ACSL1-deficient mouse model. (*A*) *Acsl1* PCR yields a 763-bp band for the WT *Acsl1* allele and a 319-bp band for the LoxP allele (*Upper*). LysM-Cre recombinase PCR yields a 350-bp band for the WT allele and a 700-bp band for the LysM Cre-recombinase allele. (*B*) Loss of *Acsl1* mRNA in thioglycollate-elicited macrophages from $ACSL1^{M-/-}$ mice. (*C*) Reduced ACSL1 protein levels in thioglycollate-elicited peritoneal macrophages from $ACSL1^{M-/-}$ mice. (*D–F*) Thioglycollate-elicited macrophages from $LDLR^{-/-}$ mice ($n = 7$–10) transplanted with bone marrow from WT or $ACSL1^{M-/-}$ mice were stained with Oil red O for neutral lipids (*D*) or used to quantify total cellular cholesterol (*E*) and total cellular triacylglycerol (*F*). The results are expressed as mean + SEM ($n = 3$ unless otherwise noted). $^{**}P < 0.01$ by unpaired Student *t* test (*B* and *C*). TG, triacylglycerol.

ACSL1 deficiency, but a significant inhibition of 18:1-induced triacylglycerol (TG) accumulation was noted in vitro (Fig. S2 *I–K*). To test whether ACSL1 deficiency reduces neutral lipid accumulation in macrophages in $LDLR^{-/-}$ mice, which have a plasma lipid profile more similar to humans than C57BL/6 mice, $LDLR^{-/-}$ mice received bone marrow transplants from WT or $ACSL1^{M-/-}$ mice. Thioglycollate-elicited macrophages from mice transplanted with $ACSL1^{M-/-}$ bone marrow exhibited the expected reduction in *Acsl1* mRNA, suggesting adequate reconstitution and chimerism. However, there were no defects in neutral lipid accumulation in these ACSL1-deficient macrophages (Fig. 3 *D–F*).

Myeloid ACSL1 Deficiency Reduces Arachidonoyl-CoA Levels and Inflammatory PGE_2 Secretion from Macrophages Under High-Glucose Conditions. We further investigated the cellular consequences of ACSL1 deficiency. ACSL1 deficiency resulted in a marked reduction in 20:4-CoA levels, whereas other acyl-CoA species were not significantly affected (Fig. 4*A*), consistent with the increased ACSL1 and increased 20:4-CoA levels in macrophages from diabetic mice (Fig. 1*P*). We next evaluated the effect of ACSL1 deficiency on arachidonic acid-derived lipid mediators (and some lipid mediators derived from other long-chain fatty acids) in macrophages subjected to normal (5.5 mM) or high (25 mM) glucose conditions by using LC-MS/MS. Macrophages differentiated in the presence of a high-glucose concentration exhibited elevated levels of PGE_2 and PGD_2 (Fig. 4*B* and Table S1). Interestingly, ACSL1 deficiency slightly but significantly blunted the increased PGE_2 and PGD_2 production in inflammatory macrophages subjected to high-glucose concentrations but not macrophages maintained in normal glucose (Fig. 4*B* and Table S1). Elevated glucose also resulted in increased levels of 15-HETE, 17-HDHA, and $PGF_{2\alpha}$, but ACSL1 deficiency had no effect on these lipid mediators or other lipid mediators under the conditions tested (Table S1).

To investigate whether the increased PGE_2 or PGD_2 levels might exert inflammatory actions in macrophages, BMDMs were differentiated in the presence or absence of 5 μM PGD_2 or PGE_2. Exogenously added PGD_2 had less of an inflammatory effect than PGE_2. Thus, we focused our subsequent studies on PGE_2. Indeed, exogenous PGE_2 stimulated IL-6 release, and this effect was enhanced under high-glucose conditions (Fig. 4*C*), possibly because of the increased endogenous PGE_2 production in glucose-stimulated cells.

To better understand the mechanism whereby high-glucose concentrations can stimulate PGE_2 production in macrophages, we analyzed mRNA levels of enzymes in the PGE_2 synthesis pathway. Elevated glucose promoted *Ptgs2* mRNA levels in M1 macrophages (Fig. 4*D*), consistent with data on macrophages from diabetic mice (Fig. 1 *E* and *L*). Similar results were obtained for microsomal *Ptges* mRNA (Fig. 4*E*), which in concert

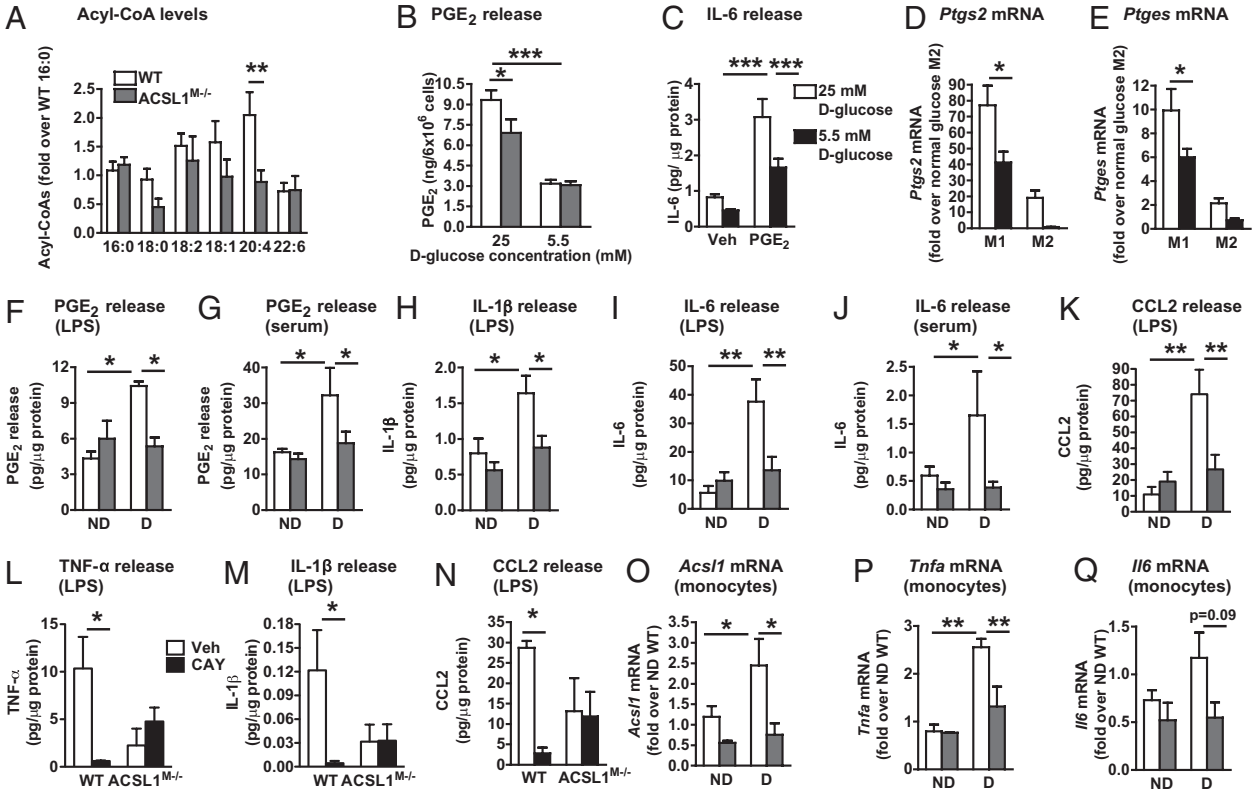

Fig. 4. ACSL1 deficiency inhibits arachidonoyl-CoA synthesis and levels of inflammatory PGE_2, cytokines, and chemokines in macrophages. (*A*) Acyl-CoA levels in thioglycollate-elicited macrophages were measured by LC-ESI-MS/MS ($n = 8$). (*B*) Levels of 20:4-derived PGE_2 ($n = 4–5$). (*C*) IL-6 release, measured by ELISA, from unactivated BMDMs differentiated in the presence or absence (control vehicle) or 5 μM PGE_2 and 25 or 5 mM D-glucose ($n = 3$). (*D* and *E*) *Ptgs2* and *Ptges* levels in WT M1 and M2 BMDMs under normal (5.5 mM) and high (25 mM)-glucose conditions were measured by real-time qPCR ($n = 3$). (*F–K*) Diabetes was induced in WT and $ACSL1^{M-/-}$ mice by streptozotocin ($n = 3–5$). After 4 wk of diabetes, thioglycollate-elicited macrophages were isolated, adhesion-purified for 1 h, and then incubated in the presence of 5 ng/mL LPS or 5% autologous serum for 6 h as indicated, or WT and $ACSL1^{M-/-}$ macrophages from diabetic mice were incubated in the presence of the PTGS2 inhibitor CAY10404 (500 nM) or vehicle (*L–N*). PGE_2 release (*F* and *G*), IL-1β release (*H* and *M*), IL-6 release (*I* and *J*), CCL2 release (*K* and *N*), and TNF-α release (*L*) were measured by ELISA. IL-1β and CCL2 release from serum-stimulated cells was below detection or 100-fold lower than in LPS-stimulated cells. (*O–Q*) Freshly isolated nonstimulated monocytes were isolated from blood of nondiabetic and diabetic WT and $ACSL1^{M-/-}$ mice after 4 wk of induction of diabetes with streptozotocin. *Acsl1* (*O*), *Tnfa* (*P*), and *Il6* (*Q*) mRNA was measured by real-time PCR. The results are expressed as mean + SEM ($n = 3–4$ unless otherwise noted). $^*P < 0.05$, $^{**}P < 0.01$, and $^{***}P < 0.001$; ANOVA.

with PTGS2, promotes production of PGE_2 from 20:4. Other enzymes involved in eicosanoid production, such as arachidonate 5- and 15-lipoxygenases or thromboxane A synthetase 1, were not elevated by glucose in M1 macrophages, but arachidonate 5-lipoxygenase was markedly elevated by glucose in M2 macrophages (Fig. S3); 19.5 mM L-glucose, used as an osmotic control, did not mimic the effect of high glucose (Fig. S3). Finally, ACSL1 deficiency did not affect peroxisome proliferator-activated receptors or liver X receptor target genes (Fig. S3), indicating that increased activity of these nuclear receptors cannot explain the effect of ACSL1 deficiency.

Together, these results suggest that increased 20:4-CoA levels, as a result of ACSL1 induction, and subsequent release of PGE_2 from macrophages in the setting of diabetes contribute to the diabetes augmented inflammatory macrophage phenotype.

Myeloid-Specific ACSL1 Deficiency Selectively Prevents the Inflammatory Phenotype of Macrophages from Diabetic Mice and Diabetes-Accelerated Atherosclerosis. Because ACSL1 expression correlates with an inflammatory macrophage phenotype in the setting of diabetes, we next investigated whether ACSL1 modulates the inflammatory response. Diabetes was induced in WT and $ACSL1^{M-/-}$ mice by streptozotocin, and 4 wk later, thioglycollate-elicited macrophages were collected, adhesion-purified, and incubated in the presence of 5% autologous serum or 5 ng/mL LPS for 6 h. Consistent with our findings in the $LDLR^{-/-}$;GP^{+} model, macrophages from diabetic mice released more PGE_2 than macrophages from nondiabetic mice, both under autologous serum and LPS stimulations, and this effect was completely prevented by ACSL1 deficiency (Fig. 4 *F* and *G*), consistent with the in vitro data (Fig. 4*B*), although the in vivo effect of ACSL1 deficiency was more marked. Diabetes also resulted in increased release of IL-1β, IL-6, chemokine (C-C motif) ligand 2 (CCL2), and TNF-α from macrophages. ACSL1 deficiency completely prevented the effect of diabetes on release of cytokines but had no effect in macrophages from nondiabetic mice (Fig. 4 *H–K*). Similarly, albeit less striking, ACSL1 deficiency reduced release of cytokines from M1 macrophages in vitro without affecting the M2 activation marker arginase 1 (Table 1). Thus, the in vitro M1 activation model does not exactly mimic the effect of diabetes on macrophages.

Together, these results suggest that ACSL1 deficiency prevents release of an inflammatory 20:4-derived lipid mediator under diabetic conditions. To directly test this hypothesis, thioglycollate-elicited macrophages were harvested from diabetic WT and $ACSL1^{M-/-}$ mice and incubated with LPS as above in the presence or absence of a selective PTGS2 inhibitor CAY10404 (500 nM). Inhibition of PTGS2 significantly reduced the production of TNF-α, IL-1β, and CCL2 in WT diabetic macrophage but had no effect on diabetic ACSL1-deficient macrophages (Fig. 4 *L–N*).

In addition, freshly isolated nonstimulated monocytes from diabetic animals displayed increased *Acsl1* expression and inflammatory markers (Fig. 4 *O–Q*), similar to what was observed in monocytes from humans with type 1 diabetes (Fig. 1*S*) (1–2). This display showed that the effect of diabetes on myeloid ACSL1 induction is not limited to peritoneal macrophages but occurs at the level of the circulating monocyte, and it is maintained as these monocytes differentiate into macrophages. Interestingly, ACSL1 deficiency prevented the diabetes-induced up-regulation of *Tnfa* and *Il6* mRNA in monocytes. These results show that ACSL1-deficient monocytes/macrophages have a markedly impaired inflammatory capacity in the setting of diabetes.

To elucidate the role of macrophage ACSL1 deficiency in diabetes-accelerated atherosclerosis, we next transplanted $LDLR^{-/-}$;GP^{+} mice with bone marrow from WT or $ACSL1^{M-/-}$ mice. Diabetic mice fed the low-fat diet previously used in this model (10) were hyperglycemic (Fig. 5*A*) but showed no significant differences in blood cholesterol levels (Fig. 5*B*) during the 12-wk study or plasma TG levels at the end of the study (Fig. 5*C*) compared with nondiabetic controls, consistent with our previous studies (10). Importantly, myeloid ACSL1 deficiency did not interfere with the onset or severity of diabetes (Fig. 5*A*), and it did not affect blood glucose, cholesterol, plasma triglycerides, or nonesterified fatty acids in diabetic or nondiabetic mice (Fig. 5 *A–C* and Table S2). There also were no statistically significant differences in markers of systemic inflammation between the four groups (Table S2), and no differences were observed in monocyte numbers or markers for neutrophils (*S100a8*) or monocyte $Ly6^{hi}$ and $Ly6^{lo}$ subsets in blood from WT and $ACSL1^{M-/-}$ mice (Fig. S3), suggesting that ACSL1 deficiency did not reduce the number of circulating monocytes or neutrophils in nondiabetic or diabetic mice. *Acsl1* mRNA levels were barely detectable in WT peritoneal neutrophils and not reduced in neutrophils from $ACSL1^{M-/-}$ mice (Fig. S3*K*). Furthermore, ACSL1 deficiency did not induce apoptosis in macrophages from nondiabetic or diabetic mice (Fig. S4*A*).

Peritoneal macrophages were harvested from a subset of bone marrow-transplanted mice 4 wk after induction of diabetes for investigation of the extent of chimerism and the proinflammatory phenotype of macrophages. As shown in Fig. 5*D*, diabetes increased *Acsl1* mRNA in macrophages from WT diabetic mice compared with WT nondiabetic mice, which was expected. Mice that had received bone marrow from $ACSL1^{M-/-}$ mice exhibited an almost complete loss of *Acsl1* mRNA and ACSL1 protein in macrophages, showing efficient chimerism. Macrophages deficient in ACSL1 were protected from diabetes-induced release of CCL2 (Fig. 5*E*) and TNF-α (Fig. 5*F*) also in this model of diabetes, consistent with the data in Fig. 4 *H–K*.

Because macrophages play a critical role in diabetes-accelerated atherosclerosis (10), formation of macrophage-rich lesions was next used as a biological endpoint to investigate the protective effect of ACSL1 deficiency in macrophages in the setting of diabetes. Analysis of Movat's pentachrome-stained cross-sections of atherosclerotic lesions in the brachiocephalic artery (BCA) revealed that diabetes increased lesion size (Fig. 5 *G–I*), as previously described (10). Interestingly, myeloid ACSL1 deficiency prevented diabetes-accelerated atherosclerosis (Fig. 5 *G–I*) by reducing macrophage accumulation (Fig. 5 *H* and *J*). However, macrophage ACSL1 deficiency did not reduce the lesion area or macrophage accumulation in nondiabetic mice (Fig. 5 *G–J*). Similar results were obtained from Sudan IV-stained aortic arches, where the lesions were larger than in the BCA (Fig. 5*K*). We next evaluated PTGS2 and CCL2 immunoreactivity in BCA lesions from the four groups of mice. Lesion PTGS2 immunoreactivity was weak but specific, and it was observed in macrophage areas (Fig. 5*L*). Lesions from diabetic WT mice exhibited more PTGS2-positive cells compared with nondiabetic mice ($P < 0.05$), whereas there was no difference between nondiabetic mice and diabetic $ACSL1^{M-/-}$ mice. Specific CCL2 immunoreactivity was detectable in macrophage-rich areas, although not all macrophages stained positive for CCL2 (Fig. 5*M*). Fewer diabetic $ACSL1^{M-/-}$ mice showed CCL2-positive lesions compared with WT diabetic mice ($P < 0.05$, Fisher exact test).

Table 1. Myeloid ACSL1 deficiency inhibits release of inflammatory mediators from LPS/IFNγ-stimulated (M1) macrophages

	WT	$ACSL1^{M-/-}$
IL-6 (ng/μg protein)	124.0 ± 0.6	58.5 ± 9.0*
TNF-α (ng/μg protein)	65.8 ± 4.1	33.0 ± 7.1†
CCL2 (ng/μg protein)	336.7 ± 17.0	262.2 ± 17.0†
Arginase 1 (arbitrary units)	0.92 ± 0.2	0.94 ± 0.1

Mean ± SEM (n = 3–6).
*$P < 0.01$ by unpaired Student t test.
†$P < 0.05$ by unpaired Student t test.

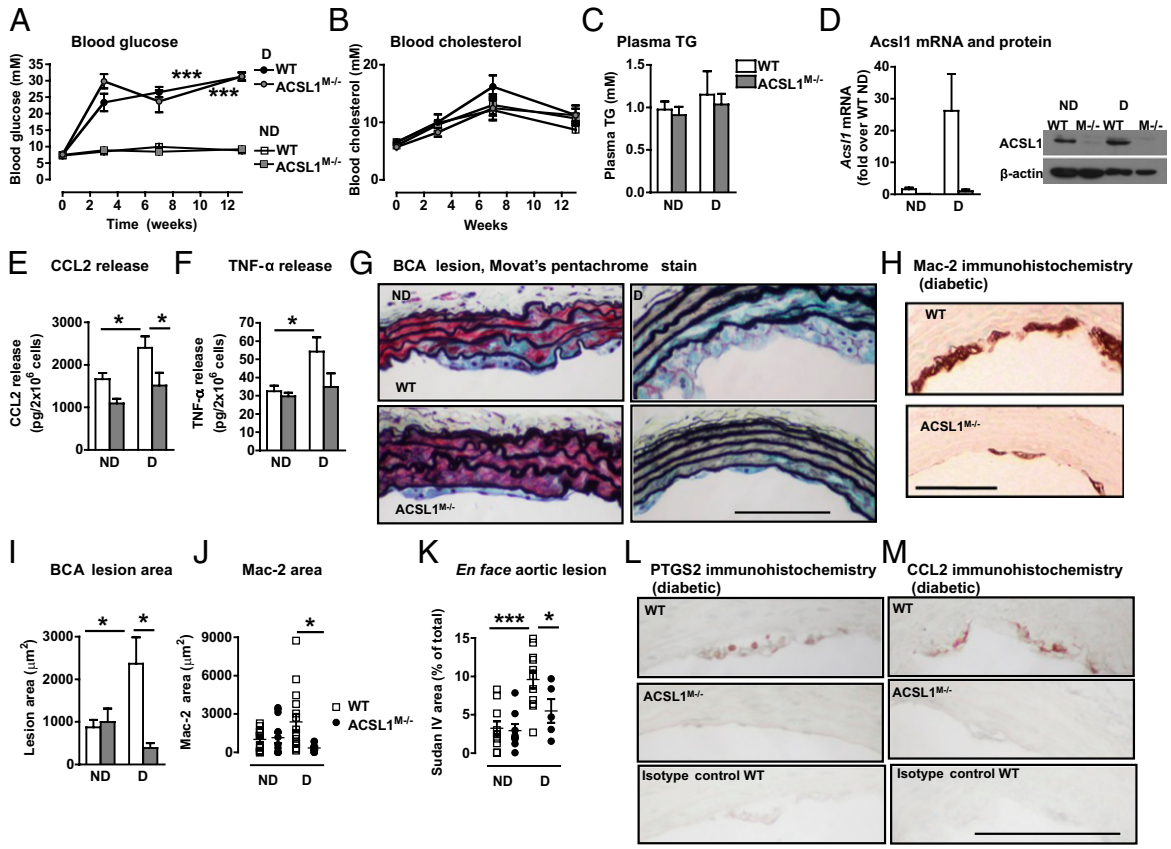

Fig. 5. Myeloid ACSL1 deficiency protects against the diabetes-induced macrophage inflammatory phenotype and atherosclerosis. Female LDLR$^{-/-}$;GP^{+} mice (12–14 wk) were bone marrow-transplanted with bone marrow from WT or ACSL1$^{M-/-}$ mice. After a 3- to 7-wk recovery period, diabetes was induced. The mice were maintained on a low-fat diet after the onset of diabetes. Blood glucose (*A*) and cholesterol (*B*) were monitored at indicated time points, and plasma TG (*C*) was measured at the end of the 12-wk study (n = 8–15). A subset (n = 5–7) of mice was euthanized after 4 wk of diabetes, and thioglycollate-elicited peritoneal macrophages were harvested by lavage. Real-time qPCR was used to determine abundance of (*D*) *Acsl1* mRNA, and Western blot was used to detect ACSL1 protein. ELISAs were used to determine levels of secreted CCL2 (*E*) and TNF-α (*F*) in the media after a 6-h incubation. After 12 wk of diabetes, the entire BCA was serial-sectioned. (*G*) Examples of Movat's pentachrome-stained cross-sections of the BCA. (*H*) Sections from diabetic animals stained using an anti–Mac-2 antibody. (*I*) The macrophage-rich lesion area was analyzed over three slides at the site of maximal lesion size for each mouse. (*J*) Quantification of Mac-2–positive lesion BCA area. (*K*) The aorta was opened longitudinally, the aortic arch was stained using Sudan IV, and the Sudan IV-positive lesion area was quantified by Image J. (*L*) Immunohistochemistry showing PTGS2 immunoreactivity in lesions from diabetic mice and an isotype-matched negative control antibody. (*M*) Immunohistochemistry showing CCL2 immunoreactivity in lesions from diabetic mice. The results are expressed as mean + SEM. *P < 0.05 and ***P < 0.001 by one-way ANOVA. (Scale bar: 100 μm.) The results are shown as mean + or ± SEM. *P < 0.05 and ***P < 0.001 by one-way ANOVA or Student t test (*F*).

To confirm that the selective protection provided by myeloid ACSL1 deficiency in diabetic mice was not because of the fact that lesions were larger in diabetic than nondiabetic mice, a group of nondiabetic mice transplanted with WT or ACSL1$^{M-/-}$ bone marrow were analyzed after 20 wk. The atherosclerotic lesions in these nondiabetic mice were of the same size as the lesions in diabetic mice at the 12-wk time point. Myeloid ACSL1 deficiency did not reduce the size of these larger lesions in nondiabetic mice (Fig. S4*B*), showing that myeloid ACSL1 deficiency selectively prevents atherosclerosis in the diabetic setting. Furthermore, myeloid ACSL1 deficiency did not reduce lesion size in hyperlipidemic nondiabetic LDLR$^{-/-}$ mice fed a high-fat diet (Fig. S4).

To investigate whether myeloid ACSL1 expression plays a role in advanced preexisting lesions, LDLR$^{-/-}$;GP^{+} mice were fed a semipurified high-fat diet for 16 wk (22) to allow advanced lesions to develop in the BCA. The mice were then switched to the low fat diet used above, transplanted with bone marrow from WT or ACSL1$^{M-/-}$ mice, injected with LCMV or saline after a recovery period, and maintained on the low fat diet for another 12 wk. Diabetes did not alter plasma lipid levels or lesion severity, consistent with our previous studies on this model in which diabetes had a detrimental effect on preexisting advanced lesions only when it was associated with elevated triglycerides (22). Diabetic mice with myeloid ACSL1 deficiency exhibited a small but significant reduction in the overall lesion severity using a combination of markers (Table S3), in these preexisting fibrotic advanced lesions (Fig. S4). However, this effect was small compared with the effect of myeloid ACSL1 deficiency on macrophage accumulation in early lesions in the setting of diabetes, perhaps because macrophages constituted only <10% of these advanced lesions.

Discussion

We show that type 1 diabetes, both in mouse models of the disease and human subjects, results in increased levels of ACSL1 in monocytes and macrophages. This increase in ACSL1 expression is associated with increased levels of 20:4-CoA and an increased PGE_2 release from macrophages from diabetic mice. We also show that inhibition of PTGS2 blocks the inflammatory macrophage phenotype associated with diabetes, showing that the inflammatory effect of diabetes is because of a PTGS2-derived lipid mediator. Of the lipid mediators analyzed in this

study, PGE_2 was identified as the most likely candidate, although we cannot rule out contribution of other PTGS2 products. Thus, PGE_2 promotes an inflammatory phenotype of mouse macrophages when these cells are exposed to PGE_2 during differentiation, consistent with recent findings in human macrophages (23). This long-term inflammatory effect of PGE_2 is different from its ability to acutely inhibit LPS-induced inflammation through EP4 receptor-associated protein (24).

Conversely, myeloid-specific ACSL1 deficiency results in a specific reduction in 20:4-CoA levels and completely prevents the increased release of PGE_2 and increased inflammatory phenotype in monocytes and macrophages from diabetic mice, showing that the increased ACSL1 expression is required for diabetes-stimulated PGE_2 release and release of inflammatory chemokines and cytokines. Furthermore, whereas PTGS2 inhibition completely blocks the inflammatory phenotype of macrophages from diabetic mice, such inhibition has no effect in ACSL1-deficient macrophages, supporting the conclusion that ACSL1 deficiency acts by reducing the PTGS2 pathway. Myeloid ACSL1 deficiency prevents the diabetes-accelerated macrophage accumulation in lesions of atherosclerosis. The selectivity of the protective effect of myeloid ACSL1 deficiency suggests that induction of a macrophage inflammatory phenotype and atherosclerosis in the setting of diabetes has an etiology that may be different from the etiology of atherosclerosis in the absence of diabetes and that one of the differences is an increased ACSL1 expression in myeloid cells. Our observations indicate that the inhibitory effect of ACSL1 deficiency on the inflammatory phenotype of macrophages associated with diabetes is likely to explain its antiatherosclerotic effects in diabetic mice and suggest that diabetes-accelerated atherosclerosis might be driven by an increased inflammatory phenotype characterized by increased ACSL1 expression in myeloid cells. Importantly, these studies identify a key step in the mechanism of diabetes-induced macrophage inflammatory changes and atherosclerosis.

The reduced macrophage accumulation in diabetic mice with myeloid ACSL1 deficiency is unlikely to be because of increased macrophage neutral lipid loading, because no defect in lipid accumulation was observed in ACSL1-deficient macrophages. Thus, myeloid-specific ACSL1 deletion in vivo is unlikely to promote cholesterol efflux, which has been shown in fatty acid-loaded macrophages in vitro (25) and results in a more specific effect than systemic inhibition of several of the ACSL isoforms using triacsin C (26). Increased macrophage death in the absence of ACSL1 is also unlikely to explain the phenotype, because no increase in macrophage apoptosis is observed in ACSL1-deficient macrophages. Furthermore, we have previously shown that, in this mouse model, macrophage proliferation within the atherosclerotic lesion is nondetectable (27), indicating that macrophage ACSL1 deficiency is unlikely to act through a reduced macrophage proliferation. Thus, the reduced lesion macrophage accumulation in mice with ACSL1-deficient macrophages is most likely because of reduced recruitment of monocytes into the lesion. Our findings that CCL2 secretion is increased from macrophages from diabetic mice and that this effect is completely prevented by ACSL1 deficiency, together with the findings that ACSL1 is up-regulated in circulating monocytes and that ACSL1 deficiency prevents diabetes-induced inflammatory changes in monocytes, support the notion that monocyte recruitment is reduced by ACSL1 deficiency. Furthermore, CCL2 immunoreactivity was reduced by myeloid ACSL1 deficiency in lesions of atherosclerosis in diabetic mice. Indeed, mice deficient in CCL2 exhibit reduced atherosclerosis concomitant with reduced lesion macrophage accumulation (28), consistent with an important role for CCL2 in atherogenesis.

What are the molecular mechanisms of the protective effects of ACSL1 deficiency on the monocyte and macrophage in the diabetic milieu? Together, our results suggest that increased release of PGE_2, perhaps in combination with other inflammatory 20:4-derived lipid mediators, from monocytes/macrophages in the setting of diabetes is likely to contribute to the augmented inflammatory phenotype. Increased release of PGE_2 has been reported previously in several cell types in response to diabetes or elevated glucose concentrations (29–31), and it has been shown to be caused by increased activity of calcium-dependent phospholipase A_2, which catalyzes the release of arachidonic acid from membrane phospholipids (30) and increases PTGS2 expression (4, 31). Our studies show that, in concert with PTGS2, prostaglandin E synthase-1 (PGES-1 or *Ptges*) is increased in macrophages exposed to elevated glucose concentrations, which is likely to contribute to the increased PGE_2 synthesis seen in macrophages from diabetic mice and macrophages exposed to elevated glucose. Indeed, an integrated omics analysis of eicosanoids and their enzymes has shown that levels of PTGS2, PGES-1, and PGE_2 are preferentially increased by inflammatory stimuli in macrophages (32), providing a likely explanation for why elevated glucose levels promote this arm of eicosanoid metabolism. There is also evidence supporting a proatherosclerotic effect of PGE_2. PGES-1–deficient mice exhibit reduced atherosclerosis and reduced macrophage accumulation in these lesions (33). These mice have significantly reduced levels of PGE_2 but also increased levels of PGI_2, which might have contributed to the atheroprotective phenotype (33).

ACSL1 deficiency, with its preferential inhibitory effect on arachidonoyl-CoA synthesis, is well-positioned to prevent diabetes-induced production of arachidonoyl-CoA and PGE_2. The reduced synthesis of arachidonoyl-CoA in ACSL1-deficient macrophages likely leads to reduced trapping of free 20:4 as arachidonoyl-CoA, resulting in a reduced pool of membrane 20:4 available as a substrate for calcium-dependent phospholipase A_2 and subsequent generation of PGE_2 resulting from the increased PGES-1 in macrophages exposed to elevated glucose. Such a model is consistent with our recent studies in other tissues (21, 34). However, we cannot rule out the possibility that ACSL1 deficiency acts in part by additional mechanisms related to the reduced synthesis of arachidonoyl-CoA or less likely, other acyl-CoAs.

Interestingly, a recent study shows that deleting toll-like receptor 2 (TLR2) prevents the inflammatory effects of diabetes on macrophages (35). In that study, whole-body TLR2 deficiency reduced increased systemic inflammation in diabetic mice, which could explain the effect on the macrophage inflammatory phenotype. In the present study, myeloid ACSL1 deficiency did not affect systemic inflammation, suggesting that the mechanisms of the reduced macrophage inflammatory phenotype in myeloid ACSL1-deficient mice and whole-body TLR2-deficient mice might be distinct. Nevertheless, a possible connection between ACSL1 and TLR2 signaling is an important topic for future research.

In summary, we show that diabetes results in an inflammatory monocyte/macrophage phenotype characterized by increased ACSL1 expression, PGE_2 release, and increased chemokine and cytokine production and that ACSL1 is critically important in mediating the increased macrophage inflammatory phenotype and atherosclerosis in diabetes. Our observations, thus, suggest a model for selective inhibition of atherosclerosis associated with diabetes.

Materials and Methods

Isolation of Monocytes, Macrophages, and Neutrophils from Nondiabetic and Diabetic Mice. The model of type 1 diabetes ($LDLR^{-/-}$;GP^+), in which diabetes can be induced at will using viral mimicry with LCMV, has been described previously (10). Adult 12- to 14-wk-old female and male $LDLR^{-/-}$;GP^+ or $LDLR^{-/-}$ mice without the GP transgene were injected with LCMV (1×10^5 pfu) or saline (control). One week after injection, at the onset of diabetes, the mice were switched to a low fat semipurified diet (10) and maintained for 4 wk. Only mice injected with LCMV and expressing the GP transgene

become diabetic. In other experiments, diabetes was induced by streptozotocin (mixed anomers no. S0130, 50 mg/kg; Sigma) dissolved immediately before use in freshly made citrate buffer (0.1 M, pH 4.5) and injected intraperitoneally for 5 consecutive d in male or female adult LDLR$^{-/-}$;GP mice or WT and ACSL1$^{M-/-}$ mice. If mice had not developed diabetes within 2 wk after the last injection, they were reinjected for another 5 d. Mice were considered diabetic if their blood glucose was 250 mg/dL or higher. One week after the last injection, the mice were switched to the low fat semipurified diet (10) and maintained for 4 wk. Diabetic mice were monitored at least biweekly for glucose, glycosuria, ketonuria, and body weight. Most LCMV-injected diabetic mice required exogenous insulin (bovine insulin implants, Lin Shin, Toronto, ON, or Lantus, Sanofi; Aventis) to prevent weight loss and ketonuria. At the end of 4 wk, thioglycollate-elicited, resident macrophages or monocytes were harvested as described below. In some experiments, the macrophages were stimulated for 6 h with LPS (5 ng/mL), autologous serum (5%), or CAY10404 (500 nM; Cayman Chemical) after isolation and a 1-h adhesion purification. Monocytes were freshly harvested from EDTA-collected blood, and erythrocytes were lysed followed by monocyte enrichment using the EasySep Mouse Monocyte Enrichment kit (Stemcell Technologies).

We initially used resident peritoneal macrophages to study the effects of diabetes to avoid the possibility that thioglycollate might mask the effects of diabetes (Fig. 1 *C*–*G*). Thioglycollate was later determined to not mask the effects of diabetes on inflammatory mediators and ACSL1, and thioglycollate-elicited macrophages were, therefore, used in all subsequent experiments because of the better yield of cells. Thioglycollate-elicited macrophages were isolated as described previously (20). Resident peritoneal macrophages were collected in the absence of thioglycollate injection. The macrophages were adherence-purified for 1 h followed by a wash with PBS to remove nonadherent cells. BMDM polarization to M1 and M2 states was performed according to the work by Odegaard et al. (19). For studies of the effect of glucose, bone marrow differentiation and activation were done in glucose-free RPMI supplemented with either 5.5 (normal) or 25 mM (high) endotoxin-free D-glucose or 5.5 mM D-glucose plus 19.5 mM L-glucose (Sigma Aldrich). During the activation, media were changed every 12 h to prevent glucose depletion.

Peritoneal neutrophils were isolated 4 h after thioglycollate injection (36). The cells were adhesion-purified, and the nonadherent cells were used for analysis of *Acsl1* mRNA levels. RNA extraction was carried out using the RNeasy Lipid Tissue kit (Qiagen).

Isolation of Monocytes from Human Subjects With and Without Type 1 Diabetes and Generation of Monocyte-Derived Macrophages. To investigate levels of *ACSL1* mRNA in monocytes from human subjects with type 1 diabetes and age-matched controls, fresh peripheral blood mononuclear cells were isolated from whole-blood samples using standard Ficoll gradients. Samples were obtained, with informed consent, from eight control and nine type 1 diabetic patients within 5 y of diagnosis through the Juvenile Diabetes Research Fund Center for Translational Research at the Benaroya Research Institute. Approval for these studies was obtained from the Institutional Review Board at Virginia Mason Medical Center. CD14^{+} monocytes were isolated from the peripheral blood mononuclear cells using two different methods. Monocytes in some cases were isolated with single-cell sorting using a FACSVantage cell sorter (BD Immunocytometry Systems). In other cases, monocytes were isolated by positive selection using Miltenyi anti-CD14 microbeads (Miltenyi Biotec). Representative samples from those latter isolations were verified for CD14^{+} content by FACS analysis. Samples were kept at 4 °C throughout the isolation procedures and then immediately harvested for RNA analysis.

Peripheral blood monocytes from healthy volunteers were isolated and differentiated into unactivated macrophages (controls) or classically activated macrophages (M1) essentially as described in the work by Martinez et al. (37). Briefly, monocytes were obtained from normal blood donor buffy coats by two-step gradient centrifugation followed by an additional step using CD14 positive selection on the Automacs. Macrophages were obtained by culturing monocytes for 7 d in RPMI 1640 (HyClone) supplemented with 10% FBS (Cellgro) and 100 ng/mL human recombinant M-CSF (R&D Systems). Classical activation of macrophages was achieved by treating the cells with LPS (100 ng/mL; InvivoGen) and human IFN-γ (20 ng/mL; R&D Systems) for 18 h.

Generation of Mice with ACSL1-Deficient Myeloid Cells (ACSL1$^{M-/-}$ Mice). Mice with myeloid-specific ACSL1 deficiency (ACSL1$^{M-/-}$ mice) were generated by interbreeding mice with the *Acsl1* exon 2 flanked by LoxP sites (*Acsl1*^{flox} mice) (21) with mice expressing Cre recombinase under control of the Lysozyme M (LysM) promoter. *Acsl1*^{flox} mice were backcrossed 10 generations onto the C57BL/6 background. LysM Cre-recombinase mice [B6.129P2-Lyz2$^{tm1(cre)Ifo}$/J] were obtained from Jackson Laboratory and further backcrossed until the 10th generation on C57BL/6. *Acsl1*^{flox} mice were bred with LysM-Cre mice to homozygozity (*Acsl1*$^{flox/flox}$Cre$^{Tg/Tg}$; ACSL1$^{M-/-}$). Pups were born at an expected Mendelian ratio. Several different controls were used, including mice without floxed *Acsl1* alleles (*Acsl1*$^{wt/wt}$Cre$^{0/0}$ and *Acsl1*$^{wt/wt}$Cre$^{Tg/Tg}$) and mice with floxed *Acsl1* alleles (*Acsl1*$^{flox/flox}$Cre$^{0/0}$). The loxP sites had no effect on *Acsl1* expression in the absence of Cre recombinase. To avoid the possibility that results could be influenced by Cre recombinase-induced toxicity, *Acsl1*$^{wt/wt}$Cre$^{Tg/Tg}$ mice were used as WT controls. ACSL1$^{M-/-}$ mice showed no increased mortality, gained weight normally, and exhibited no differences in general appearance or behavior.

Genotyping. For genotyping, duplex PCR was performed on tail biopsies to distinguish WT and *Acsl1* flox alleles with WT-specific primers (forward 5′-AGCAAGCCACATGAAGGCATGTGTG-3′, reverse 5′-AAGTGGGGGACATAGGTGCCACT-3′) and LoxP-specific primers (forward 5′-TAGAAAGTATAGGAACTTCGGCGCG-3′, reverse 5′-GCCCCTATATCACTTTTGGCGACA-3′). The resulting WT fragment is 763 bp, and the LoxP fragment is 391 bp. LysM-Cre recombinase and WT fragments were detected using primer sequences provided by Jackson Labs (oIMR3066-3068). The WT fragment is 350 bp, and the mutant fragment is ∼700 bp.

Analysis of ACSL Activity, Acyl-CoAs, Neutral Lipids, and Lipid Mediators. ACSL enzymatic activity and long-chain acyl-CoAs were measured as described previously (20, 34). The ACSL activity assay is not specific to the ACSL1 isoform, and it uses [^{3}H]-18:1 or [^{3}H]-16:0 rather than [^{3}H]-20:4 to avoid artifacts caused by fatty acid oxidation. Analysis of neutral lipids is described in *SI Materials and Methods*.

ELISAs, Apoptosis Assay, and Real-Time Quantitative PCR. IL-6, IL-1β, TNF-α, and CCL2 were measured in media from mouse macrophages using ELISA (eBioscience). PGE_2 was quantified using an ELISA from Cayman Chemical. Plasma SAA was analyzed by ELISA as previously described (38). For the noncommercially available serum amyloid A (SAA) ELISA, anti-mouse SAA (R&D Systems) was used. Apoptosis was evaluated by TUNEL using the HT titer TACS kit from Trevigen.

Total RNA was isolated using Qiagen RNeasy Mini Kits. To remove trace genomic DNA, all samples were DNase-treated. Real-time quantitative PCR (qPCR) was run in a 20-μL reaction using SYBR Green PCR Master Mix (Applied Biosystems or Fermentas) either as a one-step reaction or with a separate reverse transcription step. One-step qPCR (10 μL 2× Master Mix, 400 nM each primer, 1.0 unit Fermentas M-MuLV reverse transcriptase (RT), 0.5 unit RiboLock RNase Inhibitor) was run with PCR cycling conditions of 48 °C for 30 min, 95 °C for 10 min, and 40 cycles of 95 °C for 15 s and 60 °C for 1 min. After each assay, a dissociation curve was run to confirm specificity of all PCR amplicons. All primer reactions were also analyzed on agarose gels for correct size and the presence of a single reaction product. For two-step qPCR, the mRNA was first reverse-transcribed using the same RT but at 25 °C for 10 min followed by 42 °C for 60 min. The cDNA was then diluted, and qPCR was performed (40 cycles of 95 °C for 15 s and 60 °C for 1 min). Resulting cycle threshold (Ct) values were normalized to *Rn18s*, and the ΔΔCt method was then used to express values as fold-over control samples. All samples were run in at least duplicates, and statistical analysis was performed on $2^{-(\Delta Ct)}$ values. The primer sequences used can be obtained on request.

Western Blot Analysis and Immunohistochemistry. For protein analysis, total cell lysates (10–50 μg) were loaded onto SDS/PAGE gels, separated, and transferred onto nitrocellulose membranes. Detection was accomplished by using the following primary antibodies: ACSL1 antibody (rabbit polyclonal #4047, 1:1,000 dilution; Cell Signaling Technology), β-actin antibody (mouse monoclonal, 1:10,000 dilution; Sigma-Aldrich), p-JNK Thr183/Tyr185 antibody (mouse monoclonal #9255, 1:1,000 dilution; Cell Signaling), and total JNK antibody (rabbit polyclonal #9252, 1:1,000 dilution; Cell Signaling). HRP-conjugated secondary antibodies were used. In some experiments, macrophage cell membranes were isolated before Western blot analysis of ACSL1. In short, membrane fractions were acquired by a low-speed centrifugation followed by a high-speed centrifugation (5,000 × *g* for 2 min and 100,000 × *g* for 1 h at 4 °C, respectively). Supernatant and pellet were collected, respectively. A Mac-2 antibody (rat monoclonal, clone M3/38, 1:1,000 dilution; Cedarlane) was used as a loading control for membrane fractions.

Immunohistochemistry was performed on sections of BCA lesions adjacent to the maximal lesion site. A rat monoclonal anti–Mac-2 antibody was used to detect macrophages (22). A rabbit anti-PTGS2 polyclonal antibody (#4842, 1:200 dilution; Cell Signaling) was used to detect PTGS2-positive lesion cells,

and a rabbit polyclonal anti-CCL2 antibody (ab7202, 1:500 dilution; abcam) was used to detect CCL2-positive lesion cells. Both antibodies were used after antigen retrieval in boiling 10 mM citric acid and 0.05% Tween 20 buffer (pH 6.0) and a subsequent 30-min incubation in a Styrofoam box. Negative control antibodies were of the same subclass and concentration as the primary antibodies.

Analysis of Plasma Membrane-Associated ACSL1 by MS. Cell surface-associated proteins were isolated from mouse or human macrophages using biotinylation. After M1 or M2 activation, or no activation, of mouse and human macrophages, cell surface-associated proteins were isolated using the Pinpoint Cell Surface Protein Isolation Kit (product #89881; Pierce Biotechnology) according to the manufacturer's protocol. Briefly, cells were washed with ice-cold PBS and biotinylated for 30 min at 4 °C with gentle shaking. After quenching the reaction, the cells were washed with Tris-buffered saline (pH 7.2) containing 200 mM glutathione disulfide, and cellular lysates were prepared by sonication. Biotin-labeled proteins were isolated with NeutrAvidin (Pierce Biotechnology) resin. Eluted proteins were alkylated and digested overnight at 37 °C with sequencing-grade trypsin (1:50, wt/wt, trypsin/protein; Promega). Analysis of ACSL1-specific peptides was performed by LC-ESI-MS/MS as previously described (22). MS/MS spectra were searched against the mouse International Protein Index database (version ipi.MOUSE.fasta.20071030) or the human database (ipi.HUMAN.fasta.20100406) using the SEQUEST search engine with the following search parameters: unrestricted enzyme specificity, 3.0 atomic mass units (amu) precursor ion mass tolerance, 1.0 amu fragment ion mass tolerance, fixed Cys alkylation, and variable Met oxidation. ACSL1-specific peptides detected by LC-ESI-MS/MS were quantified by spectral counting (the total number of unique MS/MS spectra detected for ACSL1).

Lipid Mediator Lipidomics. Samples consisting of macrophages and the conditioned media combined were analyzed using an ABI Sciex Instruments 3200 Q-trap LC/MS/MS system equipped with a TurboV ionization source with a turbo ion spray probe. After solid-phase extraction (39), samples were suspended in mobile phase and injected into the HPLC component, which consisted of a Shimadzu LC20AD gradient pump with an Aglient Eclipse plus C18 (50 × 4.6 mm, 1.8 μm) column (Agilent Technologies). The column was eluted at a flow rate of 0.4 mL/min with methanol/water/acetic acid (60:40:0.01, vol/vol/v) with a gradient increasing to 100% methanol from 0 to 13.5 min. Information-dependent acquisition (IDA) used multiple reaction monitoring for each lipid mediator of interest with source parameters set as follows: ion spray voltage, −4,000 V; curtain gas, 20 U; ion source gas flow rates 1 and 2, 50 U each; temperature, 500 °C. IDA criteria were as follows: the most abundant compound was chosen to fragment with no exclusion of former target and above the threshold of 300 counts/s (cps). For enhanced product ion collision, energy was set at −25 V, with a spread of −5 V and +5 V using dynamic fill time. The mass range was 100–400 *m/z*, with a scan rate of 1,000 amu/s and a complete cycle (multiple reaction monitoring, IDA, and enhanced product ion) of ∼1 s. Lipid mediators prepared by total organic synthesis (i.e., PD1, RvD1, and RvE1) or commercial synthetic standards (i.e., PGs and LTB_4 from Cayman Chemical) were used to obtain calibration curves for quantitation. Deuterium-labeled eicosanoids d8-5S-HETE and d4-PGE_2 were used as internal standards.

Bone Marrow Transplants and Atherosclerosis Studies. Female $LDLR^{-/-}$;GP^{+} mice (12–14 wk old) received i.v. bone marrow transplants from either WT or $ACSL1^{M-/-}$ mice (5×10^6 cells; purified of erythrocytes) after lethal irradiation (10 Gy). For isolation of peritoneal macrophages, the mice were allowed to recover for 3–7 wk, and they were then switched to a low-fat semipurified diet (10) and maintained for an additional 4 wk. LDLR-deficient mice were used as recipients, because these mice have higher plasma lipid levels and thus, better mimic the atherosclerosis studies than C57BL/6 mice. For studies of diabetes-accelerated atherosclerosis, bone marrow-transplanted mice were allowed to recover for 3 wk, injected with LCMV or saline, and 1 wk after injection, switched to a low-fat semipurified diet and maintained for an additional 12 wk. Some nondiabetic mice were maintained for 20 wk. Body weights, blood glucose, and blood cholesterol were determined every 3–4 wk for the nondiabetic mice and more frequently if needed for diabetic mice. At the end of the study, mice were perfusion-fixed under physiological pressure (10). The BCA was dissected, embedded, and serial sectioned. Every fourth section was stained using a Movat's pentachrome stain procedure as described previously (22), and adjacent sections were used for immunohistochemistry. Maximal lesion areas were determined by an investigator in a masked fashion. In addition, the aortic arch and thoracic aorta (to the first intercostal artery) were dissected and stained using Sudan IV to assess en face lesion area (10). All animal studies were approved by the Institutional Animal Care and Use Committee at the University of Washington.

Statistical Analyses. Statistical analysis was performed using two-tailed unpaired Student *t* test, one- or two-way ANOVA with appropriate posthoc tests, or Fisher exact test. Probabilities of less than 0.05 were considered statistically significant. In vitro experiments were performed at least three times in independent experiments.

Additional Methods. Additional methods are described in *SI Materials and Methods*.

ACKNOWLEDGMENTS. We thank Ms. Shari Wang for analysis of plasma SAA, Ms. Angela Irwin for help with generation of human monocyte-derived macrophages, and Mr. Ricky Rualo for mouse colony management. This study was supported by the Samuel and Althea Stroum Endowed Graduate Fellowship in Diabetes Research (J.E.K.); Training Grant T32 HL07828 (to M.M.A.); a postdoctoral fellowship from the American Heart Association (Mid-Atlantic Region, to L.O.L.); Scientist Development Grant 10SDG3600027 from the American Heart Association (to L.B.); Pilot and Feasibility Grant P30 DK089507 (to L.B.); National Institutes of Health Grants HL092969 (to A.C.); HL018645 (Project 5, to T.N.W.); JDRF 25-2010-648 (to T.N.W.); DK082841 (to S.P.); DK07448 (to C.N.S.); HL092969 (Project 4, to J.W.H.); DK59935 (to R.A.C.); HL062887 (to K.E.B.); HL092969 (Project 2, to K.E.B.); HL097365 (to K.E.B.); University of North Carolina Nutrition Obesity Research Center Grant P30 DK056350; the Molecular Phenotyping Core; and Michigan Nutrition and Obesity Center Grant P30 DK089503. Virus, Molecular Genetics, and Cell Core of the Diabetes Endocrinology Research Center at the University of Washington Grant P30 DK17047 generated some real-time PCR results.

1. Devaraj S, et al. (2006) Increased monocytic activity and biomarkers of inflammation in patients with type 1 diabetes. *Diabetes* 55:774–779.
2. Bradshaw EM, et al. (2009) Monocytes from patients with type 1 diabetes spontaneously secrete proinflammatory cytokines inducing Th17 cells. *J Immunol* 183:4432–4439.
3. Litherland SA, et al. (1999) Aberrant prostaglandin synthase 2 expression defines an antigen-presenting cell defect for insulin-dependent diabetes mellitus. *J Clin Invest* 104:515–523.
4. Shanmugam N, Gaw Gonzalo IT, Natarajan R (2004) Molecular mechanisms of high glucose-induced cyclooxygenase-2 expression in monocytes. *Diabetes* 53:795–802.
5. Natarajan R, Nadler JL (2004) Lipid inflammatory mediators in diabetic vascular disease. *Arterioscler Thromb Vasc Biol* 24:1542–1548.
6. Jagannathan-Bogdan M, et al. (2011) Elevated proinflammatory cytokine production by a skewed T cell compartment requires monocytes and promotes inflammation in type 2 diabetes. *J Immunol* 186:1162–1172.
7. Burke AP, et al. (2004) Morphologic findings of coronary atherosclerotic plaques in diabetics: A postmortem study. *Arterioscler Thromb Vasc Biol* 24:1266–1271.
8. Nathan DM, et al. (2005) Intensive diabetes treatment and cardiovascular disease in patients with type 1 diabetes. *N Engl J Med* 353:2643–2653.
9. Gerrity RG, Natarajan R, Nadler JL, Kimsey T (2001) Diabetes-induced accelerated atherosclerosis in swine. *Diabetes* 50:1654–1665.
10. Renard CB, et al. (2004) Diabetes and diabetes-associated lipid abnormalities have distinct effects on initiation and progression of atherosclerotic lesions. *J Clin Invest* 114:659–668.
11. Vikramadithyan RK, et al. (2005) Human aldose reductase expression accelerates diabetic atherosclerosis in transgenic mice. *J Clin Invest* 115:2434–2443.
12. Bornfeldt KE, Tabas I (2011) Insulin resistance, hyperglycemia, and atherosclerosis. *Cell Metab* 14:575–585.
13. Wen Y, et al. (2006) Elevated glucose and diabetes promote interleukin-12 cytokine gene expression in mouse macrophages. *Endocrinology* 147:2518–2525.
14. Hummasti S, Hotamisligil GS (2010) Endoplasmic reticulum stress and inflammation in obesity and diabetes. *Circ Res* 107:579–591.
15. Chiu HC, et al. (2001) A novel mouse model of lipotoxic cardiomyopathy. *J Clin Invest* 107:813–822.
16. Li LO, et al. (2006) Overexpression of rat long chain acyl-coa synthetase 1 alters fatty acid metabolism in rat primary hepatocytes. *J Biol Chem* 281:37246–37255.
17. Parkes HA, et al. (2006) Overexpression of acyl-CoA synthetase-1 increases lipid deposition in hepatic (HepG2) cells and rodent liver in vivo. *Am J Physiol Endocrinol Metab* 291:E737–E744.
18. Saraswathi V, Hasty AH (2009) Inhibition of long-chain acyl coenzyme A synthetases during fatty acid loading induces lipotoxicity in macrophages. *Arterioscler Thromb Vasc Biol* 29:1937–1943.
19. Odegaard JI, et al. (2008) Alternative M2 activation of Kupffer cells by PPARdelta ameliorates obesity-induced insulin resistance. *Cell Metab* 7:496–507.
20. Askari B, et al. (2007) Rosiglitazone inhibits acyl-CoA synthetase activity and fatty acid partitioning to diacylglycerol and triacylglycerol via a peroxisome proliferator-activated receptor-γ-independent mechanism in human arterial smooth muscle cells and macrophages. *Diabetes* 56:1143–1152.
21. Ellis JM, et al. (2010) Adipose acyl-CoA synthetase-1 directs fatty acids toward beta-oxidation and is required for cold thermogenesis. *Cell Metab* 12:53–64.

22. Johansson F, et al. (2008) Type 1 diabetes promotes disruption of advanced atherosclerotic lesions in LDL receptor-deficient mice. *Proc Natl Acad Sci USA* 105: 2082–2087.
23. Hertz AL, et al. (2009) Elevated cyclic AMP and PDE4 inhibition induce chemokine expression in human monocyte-derived macrophages. *Proc Natl Acad Sci USA* 106: 21978–21983.
24. Takayama K, Sukhova GK, Chin MT, Libby P (2006) A novel prostaglandin E receptor 4-associated protein participates in antiinflammatory signaling. *Circ Res* 98:499–504.
25. Kanter JE, Tang C, Oram JF, Bornfeldt KE (2011) Acyl-CoA synthetase 1 is required for oleate and linoleate mediated inhibition of cholesterol efflux through ATP-binding cassette transporter A1 in macrophages. *Biochim Biophys Acta*, Oct. 12 [Epub ahead of print].
26. Matsuda D, et al. (2008) Anti-atherosclerotic activity of triacsin C, an acyl-CoA synthetase inhibitor. *J Antibiot (Tokyo)* 61:318–321.
27. Lamharzi N, et al. (2004) Hyperlipidemia in concert with hyperglycemia stimulates the proliferation of macrophages in atherosclerotic lesions: Potential role of glucose-oxidized LDL. *Diabetes* 53:3217–3225.
28. Combadière C, et al. (2008) Combined inhibition of CCL2, CX3CR1, and CCR5 abrogates Ly6C(hi) and Ly6C(lo) monocytosis and almost abolishes atherosclerosis in hypercholesterolemic mice. *Circulation* 117:1649–1657.
29. Schambelan M, et al. (1985) Increased prostaglandin production by glomeruli isolated from rats with streptozotocin-induced diabetes mellitus. *J Clin Invest* 75:404–412.
30. Xia P, Kramer RM, King GL (1995) Identification of the mechanism for the inhibition of Na+,K(+)-adenosine triphosphatase by hyperglycemia involving activation of protein kinase C and cytosolic phospholipase A2. *J Clin Invest* 96:733–740.
31. Koya D, et al. (1997) Characterization of protein kinase C beta isoform activation on the gene expression of transforming growth factor-beta, extracellular matrix components, and prostanoids in the glomeruli of diabetic rats. *J Clin Invest* 100: 115–126.
32. Buczynski MW, Dumlao DS, Dennis EA (2009) Thematic Review Series: Proteomics. An integrated omics analysis of eicosanoid biology. *J Lipid Res* 50:1015–1038.
33. Wang M, et al. (2006) Deletion of microsomal prostaglandin E synthase-1 augments prostacyclin and retards atherogenesis. *Proc Natl Acad Sci USA* 103:14507–14512.
34. Golej DL, et al. (2011) Long-chain acyl-CoA synthetase 4 modulates prostaglandin E_2 release from human arterial smooth muscle cells. *J Lipid Res* 52:782–793.
35. Devaraj S, et al. (2011) Knockout of toll-like receptor-2 attenuates both the proinflammatory state of diabetes and incipient diabetic nephropathy. *Arterioscler Thromb Vasc Biol* 31:1796–1804.
36. Averill MM, et al. (2011) S100A9 differentially modifies phenotypic states of neutrophils, macrophages, and dendritic cells: Implications for atherosclerosis and adipose tissue inflammation. *Circulation* 123:1216–1226.
37. Martinez FO, Gordon S, Locati M, Mantovani A (2006) Transcriptional profiling of the human monocyte-to-macrophage differentiation and polarization: New molecules and patterns of gene expression. *J Immunol* 177:7303–7311.
38. Subramanian S, et al. (2008) Dietary cholesterol worsens adipose tissue macrophage accumulation and atherosclerosis in obese LDL receptor-deficient mice. *Arterioscler Thromb Vasc Biol* 28:685–691.
39. Serhan CN, Lu Y, Hong S, Yang R (2007) Mediator lipidomics: Search algorithms for eicosanoids, resolvins, and protectins. *Methods Enzymol* 432:275–317.